JOURNAL OF SPACECRAFT AND ROCKETS
Vol. 41, No. 4, July–August 2004

North Star Plasma-Jet Space Experiment

R. E. Erlandson,* C. I. Meng,† P. K. Swaminathan,‡ C. K. Kumar,§ V. K. Dogra,¶ and B. J. Stoyanov**
Johns Hopkins University, Applied Physics Laboratory, Laurel, Maryland 20723
B. G. Gavrilov,†† Y. Kiselev,‡‡ and J. I. Zetzer§§
Institute for Dynamics of Geospheres, 117979, Moscow, Russia
H. C. Stenbaek-Nielsen¶¶
University of Alaska/Geophysical Institute, Fairbanks, Alaska 99775-7320
K. A. Lynch***
Dartmouth College, Hanover, New Hampshire 03755
R. F. Pfaff†††
NASA Goddard Space Flight Center, Greenbelt, Maryland 20771
P. A. Delamere‡‡‡
University of Colorado, Boulder, Colorado 80309
S. Bounds§§§
University of Iowa, Iowa City, Iowa 52242
and
N. A. Gatsonis¶¶¶
Worcester Polytechnic Institute, Worcester, Massachusetts 01609

The objective of the Active Plasma Experiment North Star mission was to study the interaction of artificially produced aluminum ion plasma jets with the space environment. Two separate plasma jets were injected almost perpendicular to the local magnetic field during the North Star experiment. The jets were created using an explosive-type generator designed to produce a high-speed (7–42-km/s) aluminum ion plasma jet with plasma densities exceeding 10^9 cm^{-3} at a distance 170 m from the plasma-jet source. The first plasma-jet injection occurred at an altitude of 360 km and was preceded by the release of an artificial air cloud. The second injection occurred at an altitude of 280 km and did not include the air cloud. Interactions of the plasma jet with the local space environment and artificial air cloud were monitored using instrumentation on three diagnostic payloads, ground-based optical sensors, and space-based optical sensors. An overview is provided of the experiment, along with a summary of the principal results from the mission.

Received 19 October 2001; revision received 17 December 2002; accepted for publication 3 May 2003.

*Group Supervisor, Space Department, 11100 Johns Hopkins Road. Member AIAA.
†Branch Supervisor, Space Department, 11100 Johns Hopkins Road. Member AIAA.
‡Principal Professional Staff, Space Department, 11100 Johns Hopkins Road. Member AIAA.
§Physicist, Space Department, 11100 Johns Hopkins Road. Member AIAA.
¶Senior Professional Staff, Space Department, 11100 Johns Hopkins Road. Member AIAA.
**Senior Professional Staff, Space Department, 11100 Johns Hopkins Road.
††Head, Laboratory of the Magnetosphere-Earth Coupling, 38 Leninsky Prospect.
‡‡Senior Scientist, Laboratory of the Magnetosphere-Earth Coupling, 38 Leninsky Prospect.
§§Deputy Director, 38 Leninsky Prospect.
¶¶Professor, Physics Department.
***Assistant Professor of Physics and Astronomy, Department of Physics and Astronomy.
†††Space Scientist, Goddard Space Flight Center, Code 696.
‡‡‡Research Scientist, Laboratory for Atmospheric and Space Physics.
§§§Research Scientist.
¶¶¶Associate Professor, Mechanical Engineering Department, 100 Institute Road. Senior Member AIAA.

Nomenclature

$\boldsymbol{B}$ = magnetic field vector
$\boldsymbol{E}$ = electric field vector
N = plasma density

Subscript

i = ion

Introduction

HIGH-SPEED plasma-jet experiments have been conducted in the ionosphere and magnetosphere because of their importance to the understanding of current coupling phenomena, plasma instabilities, and, in general, the electrodynamic interactions of plasma beams with magnetic fields. In addition to their importance to our understanding of basic plasma phenomena, plasma-jet experiments provide the ability to study the local spacecraft environment induced by the release of plasmas during spacecraft operations. The artificial high-speed plasma jets produced during the Active Plasma Experiment North Star mission are similar to plasma jets (or plumes) produced as a result of onboard electric propulsion thrusters or the release of neutrals and/or plasma from spacecraft subsystems. In fact, plasma plumes from electric propulsion thrusters and other active systems affect spacecraft in a number of ways. Investigations of electric propulsion plumes have focused so far on the near-field effects associated with meter-size scales, and they have considered issues related to plume backflow, contamination, and spacecraft charging.[1] However, plasma plumes induced through interactions with the ambient magnetized plasma far-field effects are associated with hundred-meter to kilometer size scales. Such interactions can

produce unwanted particle fluxes, electromagnetic perturbations, and optical backgrounds that could affect sensors onboard neighboring spacecraft, such as envisioned satellite constellations or formation-flying missions. The North Star mission comprehensively addressed the various types of far-field interactions of high-speed (7–42-km/s) plasma jets with the ambient magnetized plasma.

In the North Star mission, we used a controlled and calibrated aluminum plasma-jet source known as an explosive-type generator (ETG).[2] The ETG, similar to shaped-charge generators, used high explosives to vaporize porous aluminum that is in turn ejected from a nozzle prior to the expulsion of debris or contaminants from the high explosives. The device generates a plasma jet without the aid of solar illumination, making it possible to use optical (visible-wavelength) sensors to study the ionization, recombination, and interactions of the jet with the atmosphere and ionosphere.

We review important features of high-speed plasma-jet experiments that are relevant to the North Star mission. During the Porcupine experiment,[3] a xenon ion plasma jet, generated periodically from a plasma generator, was injected into the ionospheric plasma approximately perpendicular to the magnetic field. Measurements were acquired at distances between 1 and 1000 m using diagnostic payloads deployed from the spinning plasma-jet payload. The diagnostic payload measurements acquired within 10 m of the source, when the jet density was large, are the most relevant to the North Star experiments. The propagation of the dense plasma jet has been separated into different phases that include a diamagnetic phase, a magnetic diffusion phase, and a single-particle-motion phase.[3] In the first diamagnetic phase the plasma pressure of the jet is much greater than the magnetic field pressure resulting in the expulsion of the magnetic field from the jet. The second phase is a transitional phase, where the magnetic field diffuses into the jet. During these two phases, the jet propagates across magnetic field lines, with a velocity controlled by the electrodynamic coupling of the jet with the ambient magnetic field. The final stage occurs as the jet ions follow trajectories based on single-particle equations of motion where collective plasma effects are not present.

A series of active plasma jet experiments known as the Argon Release for Controlled Studies[4] was used to study plasma-jet neutralization,[5] plasma wave generation,[6] and ion acceleration.[7] In these experiments, the beam density was less than the ionospheric density, except near the plasma generator, and yet significant perturbations were observed in the properties of the background plasma and wave environment.

A series of barium releases was used during the Critical Ionization Tests (CRIT) I and II campaigns.[8] In CRIT, a shaped-charge device was used to inject a high-speed stream of barium neutrals roughly perpendicular to the magnetic field. Observations of ion and electron distributions were found to be consistent with those levels expected with the critical ionization velocity (CIV) process and the ionization shutoff once the velocity of the neutrals fell below the critical velocity.[8] On the other hand, Swenson et al.[9] concluded that the amount of barium ionization could be explained by a (Ba, O^+) charge exchange process.

Aluminum plasma jets similar to those of the North Star mission were produced in two nearly identical experiments, known as the Fluxus 1 and Fluxus 2.[10] The Fluxus plasma jets with energy of 3 MJ were injected nearly parallel to the magnetic field in the low-latitude ionosphere at an altitude of 140 km. The jets were directed toward a diagnostic payload separated from the ETG by 130 m at the time of the ETG detonation. The plasma jet density observed on the diagnostic payload exceeded 10^9 cm^{-3} and produced a 50% reduction of the local magnetic field through the diamagnetic effect.[11] The Midcourse Space Experiment (MSX) satellite observed the plasma jet injection using a suite of ultraviolet and visible imagers and spectrographic imagers.[12] The spectra observed using MSX were dominated by aluminum line emissions, as expected, although other lines characteristic of natural auroral and airglow emissions were also observed, presumably generated by a flux of electrons responsible for plasma jet neutralization.[13]

The North Star mission[14] was designed to study the far-field effects of high-speed plasma jets on the space environment. The goals of the North Star mission were to address, through data analysis and modeling, issues relating to the propagation of high-speed plasma jets across magnetic field lines, to investigate the role of the neutral atmosphere in secondary jet ionization processes, and to assess the CIV hypothesis. In this paper we provide an overview of the experiment and present principal results from the experiment.

Experiment Overview

The North Star mission was launched at 1358:03 UT on 22 January 1999 using a Black Brant XII sounding rocket from Poker Flat, Alaska. Launch occurred just after an auroral breakup, with the rocket crossing auroral arcs on the upward part of the trajectory prior to the execution of the active jet experiments. The active experiments included two separate plasma-jet injections (Fig. 1). The first plasma-jet experiment (ETG-1) occurred near apogee at an altitude of 360 km, and the second plasma-jet experiment (ETG-2) occurred on the downward trajectory at an altitude of 280 km (Table 1). A canister of compressed air was released prior to the first plasma-jet experiment to investigate the role of the neutral atmosphere on jet ionization and to connect the results to the previous Fluxus experiments,[10,11] conducted at 150-km altitude.

Explosive-Type Generators (Plasma-Jet Source)

The ETGs were designed to produce a high-density Al^+ plasma jet with ion velocities between 7 and 42 km/s without the aid of solar illumination.[2] Note that the ETG will produce a high-speed jet of both neutral and ionized aluminum. The neutral aluminum is formed from the rapid recombination of aluminum ions formed at the time of the ETG detonation. Laboratory tests of the ETG indicate that 90% of the plasma jet mass is contained within 20 deg of the jet axis. A schematic of the device is shown in Fig. 2. Products of the shaped-charge explosion are isolated from the aluminum jet through the design of the exit orifice. The pure aluminum spectral properties were confirmed in ground chamber tests. The absence of contaminant products associated with the shaped-charge lining was confirmed during the previous Fluxus experiment using spectral observations from the MSX satellite from 110 to 900 nm (Ref. 13). The ETG devices and the payloads containing the ETGs are destroyed by the 9.7 kg of high explosives. The debris resulting from fragmentation of the payload expands more slowly than the plasma jet and thus does not interfere with the in situ observations.

One objective of the North Star experiments was to investigate the role of the neutral atmosphere in plasma-jet ionization processes. To accomplish this objective, approximately 12 g of compressed air was released 0.2 s prior to the ETG-1 jet injection to simulate conditions found in lower altitudes. We estimated that the artificial air cloud was 150 m in extent at the time of the ETG-1 injection and had a density from 2×10^{11} cm^{-3} (at 10 m from the ETG) to 2×10^{10} cm^{-3} (at 150 m from the ETG). This can be compared with an ambient density of only 1.6×10^8 cm^{-3} at 360-km altitude (ETG-1 altitude without air canister release), 9.5×10^8 cm^{-3} at 280 km (ETG altitude), and 5×10^{10} cm^{-3} at 150-km altitude (Fluxus[10,11] altitude). An artificial air cloud was not generated during the ETG-2 injection, and so we could study the effect of the neutral atmosphere. It was our expectation that the increase in neutral density would enhance the production of the jet ionization. The North Star mission indeed demonstrated that the density of the neutral atmosphere significantly increased the plasma-jet ionization.

Table 1 Time and location of plasma-jet injections

Parameter	ETG-1	ETG-2
Time of detonation, s	345.137	500.15
Altitude, km	363	280
Geographic latitude, °	69.0	71.0
Geographic longitude, °	−148.3	−148.6

Table 2 Distance from plasma-jet source

Injection/payload	ETG-2, m	PDP, m	OSP, m
ETG-1 injection/ETG-1	170	470	1020
ETG-2 injection/ETG-1	——	540	1600

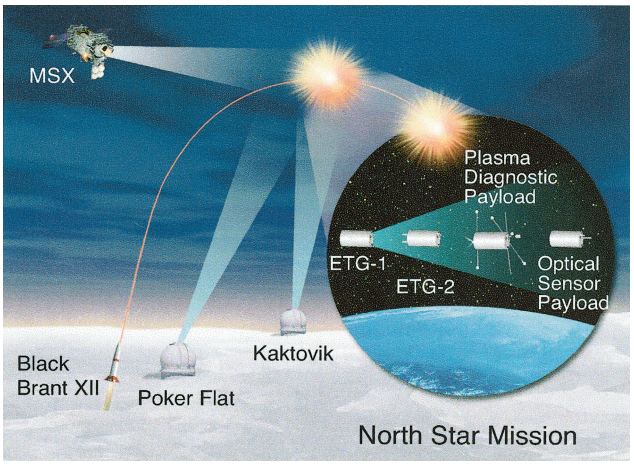

Fig. 1 North Star flight scenario.

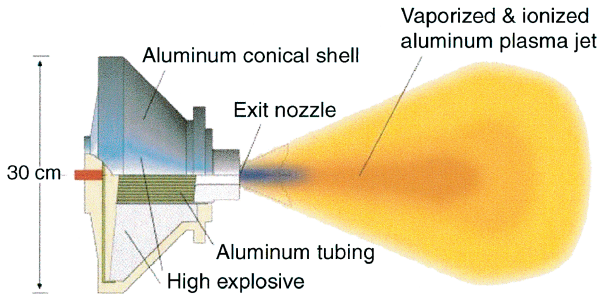

Fig. 2 Sketch of the North Star ETG.

Payload Geometry

The payloads were deployed perpendicular to the magnetic field prior to the plasma jet injections (Fig. 1). The four payloads are referred to as the ETG-1 payload, ETG-2 payload, the plasma diagnostic payload (PDP), and the optical sensor payload (OSP). The separation distances of the payloads were determined using global-positioning-system receivers on each payload (Table 2). The distances quoted in Table 2 are accurate to within ± 10 m. The orientation of the plasma-jet injections was determined using magnetometers on the ETG-1 and ETG-2 payloads and gyros during the interval of the flight while the payloads were attached to the OSP. The data indicate that the plasma jet was injected toward the diagnostic payloads during both injections. The spin axes of the diagnostic payloads (ETG-2, PDP, and OSP) were pointed to within 10 deg of the ETG-1 payload during ETG-1. During ETG-2, the spin axis of the OSP was pointed toward the ETG-2 payload, while the PDP spin axis was pointed 60 deg away from the ETG-2 payload. Furthermore, both jets were injected perpendicular to the magnetic field, to within ± 10 deg.

In Situ (Payload) Instrumentation

The North Star payloads contained a complete set of diagnostic sensors located at different distances from the plasma jet source (see Table 3 for summary). The ETG-1 payload contained one ETG and did not contain diagnostic sensors because the payload is destroyed at the time of detonation. The ETG-2 payload contained one ETG, Langmuir probes, magnetometers, ultraviolet and visible photometers, and pyroelectric sensors. The PDP contained Langmuir probes, magnetometers, ultraviolet and visible photometers pointing both toward and away from the jet, pyroelectric sensors, dc electric field receivers, plasma wave receivers, ion electrostatic analyzers, and electron electrostatic analyzers. The OSP contained a Langmuir probe, magnetometer, ultraviolet and visible spectrograph, ultraviolet and visible photometers, and infrared radiometers.

Table 3 North Star instrumentation (dynamic range and rate)

Instrument	ETG-2	PDP	OSP
Magnetic field	$\pm$100,000 nT (50 kHz) $\pm$1,000 nT (50 kHz) $\pm$70,000 nT (2.5 kHz)	$\pm$100,000 nT (50 kHz) $\pm$70,000 nT (2.5 kHz)	$\pm$70,000 nT (3.125 kHz)
Langmuir probe	10^9–10^{12} cm^{-3} (100 kHz) 10^5–10^9 cm^{-3} (10 kHz)	10^8–10^{11} cm^{-3} (100 kHz) 10^4–10^8 cm^{-3} (10 kHz) 10^4–10^8 cm^{-3} (5 kHz)	10^4–10^8 cm^{-3} (780 kHz)
Pyroelectric sensors	0.01–50 μm (100 kHz)	0.01–50 μm (50 kHz) 0.2–4 μm (50 kHz) 0.11–8 μm (10 kHz)	——
Electric fields	——	$\pm$417 mV/m (20 kHz) $\pm$1.6 V/m (20 kHz)	——
Plasma waves (δE)	——	$\pm$208 mV/m (0–128 kHz) $\pm$0.4–800 mV/m (2.5 MHz) $\pm$25 mV/m (12.5 MHz)	——
Ion detector (ESA)	——	3–200 eV (6.4 ms/sweep)	——
e–detector (ESA)	——	2 eV–2 keV (6.4 ms/sweep) 0.01–10 keV (12.8 ms/sweep)	——
Photometers (looking toward jet)	380–420 nm (30 kHz) 290–350 nm (30 kHz)	380–420 nm (50 kHz) 290–350 nm (10 kHz)	360–420 nm (6.25 kHz) 234–274 nm (50 kHz) 301–326 nm (50 kHz) 290–350 nm (6.25 kHz) 330–370 nm (6.25 kHz) 380–420 nm (50 kHz) 700–800 nm (50 kHz) 400–1,000 nm (6.25 kHz)
Photometer (looking away)	——	380–420 nm (10 kHz) 290–350 nm (10 kHz)	——
Radiometers	——	——	1.539–1.689 μm (6250 Hz) 2.55–3.02 μm (6250 Hz) 2.682–2.742 μm (6250 Hz) 4.14–4.41 μm (6250 Hz) 2.95–3.60 μm (780 Hz) 7.3–9.3 μm (780 Hz)
Spectrographs	——	——	190–410 nm (190 Hz) 380–768 nm (190 Hz)

Table 4 North Star ground-based sensors

Instrument	Location	Wavelength	Rate	Field of view, deg
Visible camera				
ICCD	Poker Flat	Visible	30 Hz	12×16
ICCD	Kaktovik	Visible	30 Hz	12×16
ICCD (conjugate)	Kaktovik	Visible	30 Hz	12×16
SIT	Poker Flat	Visible	60 Hz	12×16
High-speed photometer	Poker Flat	Visible	100 kHz	5
TV spectrograph	Poker Flat	390–800, $\Delta\lambda = 3$ nm	0.1–8 s	0.5×8
Imaging spectrograph	Poker Flat	390–800, $\Delta\lambda = 3$ nm	1–30 s	FOV: 1–180
High-speed digital imager	Kaktovik	Visible	1000 Hz	FOV: 7×7

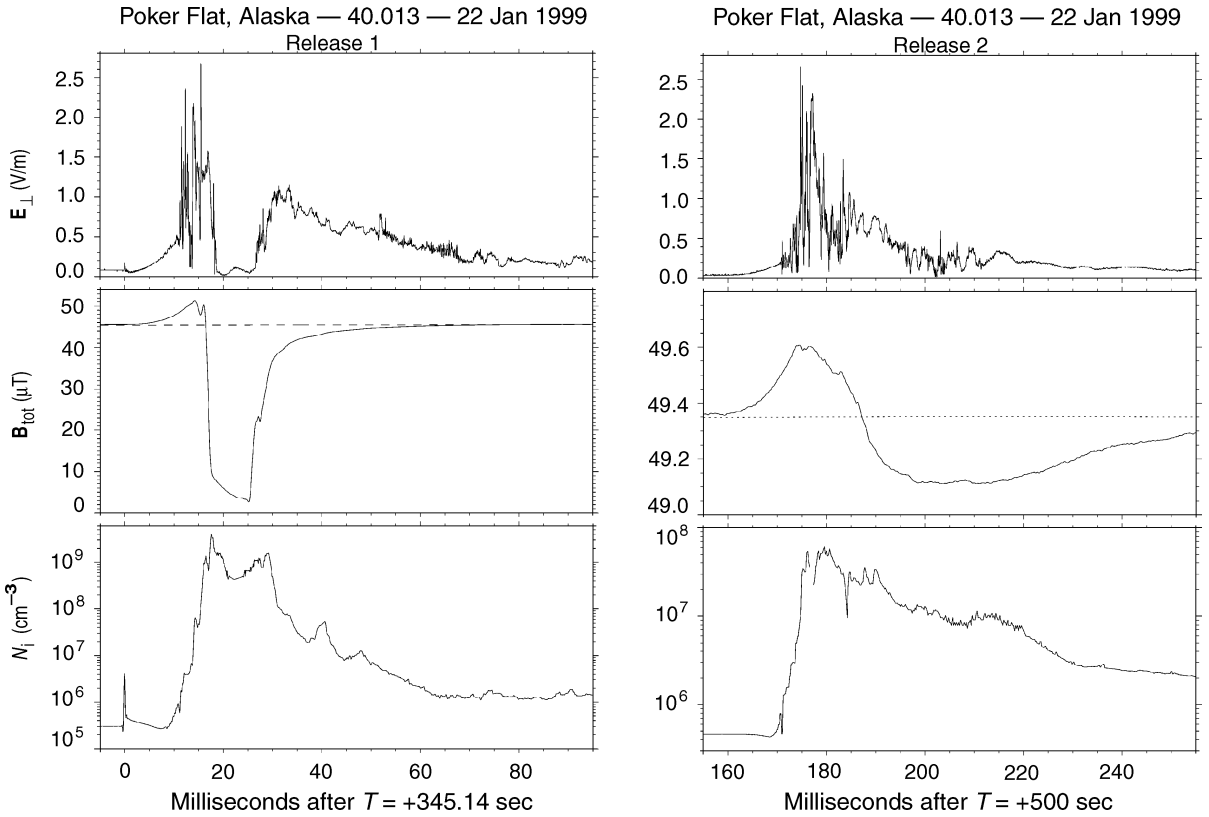

Fig. 3 PDP electric field component perpendicular to the magnetic field, total magnetic field strength, and plasma density during the first (left-hand panel) and second (right-hand panel) plasma-jet injection.

Remote Instrumentation

The optical emissions from the plasma jet were recorded using visible cameras located at Poker Flat and down-range at Kaktovik, Alaska (Table 4). The primary instruments at Poker Flat included visible imagery and high-speed photometry. At Kaktovik, a high-speed camera (1000 frames/s) and a slower-rate camera were used to observe the jet. An additional camera at Kaktovik was used to observe the ionospheric footprint of the plasma-jet injection to find out if a plasma-jet injection will produce auroral emissions. Finally, ground magnetometers were used to assess the magnetic perturbations that can result from the ETG injection.

The MSX satellite, which was in a 900-km polar circular orbit, was used to observe the North Star experiment. The satellite was located 2800 km to the east during Injection 1 and 2500 km to the east during Injection 2 and contained visible and ultraviolet sensors that included four imagers and five spectrographic imagers.[15] The spectrographic imagers provided spectral coverage from 120 to 900 nm in over 1000 bands.

Summary of Observations

Plasma Density

The plasma density of the jet was recorded using Langmuir probes on the ETG-2, PDP, and OSP payloads during the first plasma-jet injection (ETG-1) and on the PDP and OSP payloads during the second plasma-jet injection (ETG-2). As indicated in Table 3, the two different Langmuir probes were included on the ETG-2 payload, and three probes were included on the PDP payload in order to span a wide dynamic range. The Langmuir probes were held at a fixed voltage in the ion saturation regime during the plasma-jet injections. Figure 3 (bottom-left panel) shows the plasma density recorded during the ETG-1 injection at the location of the PDP payload, separated from the plasma jet source by 470 m. Data from two Langmuir probes were combined to provide a complete view of the plasma density during the passage of the ETG-1 plasma jet. The plasma density reached values four orders of magnitude above ambient levels (see density prior to 345.14 s). During the first injection, a peak plasma jet density of 3×10^9 cm^{-3} was observed. The plasma density recorded during the second injection (ETG-2) at the location of the PDP payload (now at a distance of 540 m from the plasma jet source) is shown in Fig. 3 (bottom-right panel). The peak plasma jet density during the second injection was 6×10^7 cm^{-3}. This is much smaller than the plasma-jet density recorded during the first injection. The duration of the plasma-jet passage, as inferred from the jet density, at the PDP location was similar during both injections.

The primary difference between the two plasma-jet injections was that neutral gas (compressed air) was released just prior to

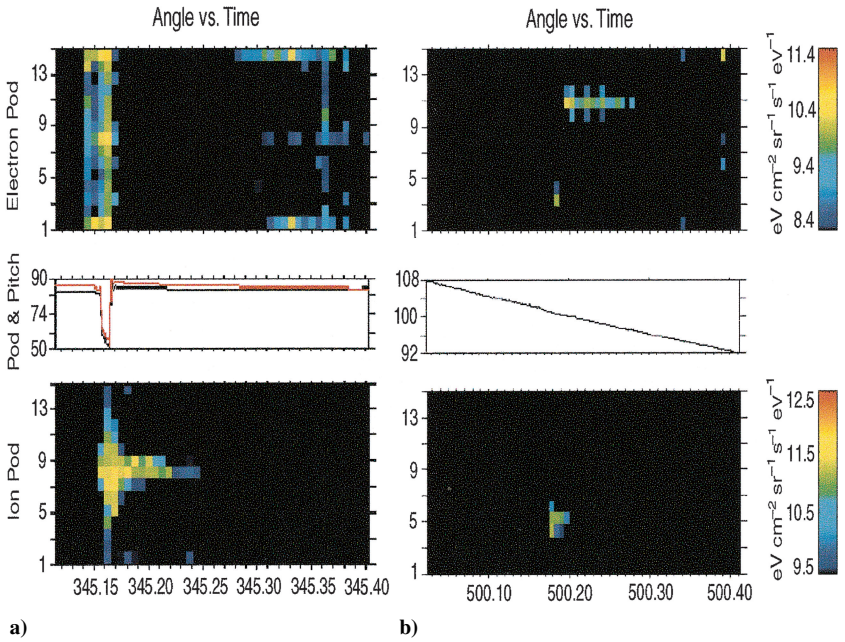

Fig. 4 Ion and electron pitch angle distribution over all energies during injection 1 (left) and injection 2 (right).

the first injection. As suggested by Gavrilov et al.,[16] the air cloud enhances the ionization of the jet, producing the enhanced plasma jet density levels during the first injection. Another possibility is that the direction of the second release was slightly displaced from the direction between the second release canister and the PDP payload.

The relative timing of the plasma-jet arrival with respect to the release was determined for the first release by noting that a small spike in the Langmuir-probe current was observed at the time of the ETG detonation (Fig. 3). This spike corresponded to the onset of visible and ultraviolet radiation. The spike in the Langmuir-probe current was most likely the result of intense ultraviolet radiation, although it could also have been caused by an electromagnetic wave generated at the time of the plasma-jet injection to which the Langmuir probe was sensitive. The absence of such a release signature on the second release is presently not understood.

Magnetic and Electric Fields

The plasma jet produced a significant reduction in the magnetic field as a result of a diamagnetic effect during the ETG-1 injection, as shown in Fig. 3 (middle-left panel). The plasma jet energy density based on PDP magnetic field data is between 10^9 and 10^{10} eV/cm^3. Assuming an electron temperature of 1 eV, the plasma density needed to produce such an effect would be $\sim 10^9$ to 10^{10} cm^{-3}, which is consistent with the Langmuir-probe observations. A similar effect was observed during the Fluxus 1 and 2 experiments.[11] In addition, an enhancement in the magnetic field was observed in front of the jet. This is possibly a result of a "snowplow" effect, where magnetic field lines are concentrated in front of the jet or a magnetosonic wave.

A diamagnetic cavity was not detected at the PDP or the OSP during ETG injection 2 (Fig. 3, right-middle panel). The lack of a diamagnetic cavity is consistent with the lower plasma-jet densities measured by the Langmuir probes during Injection 2.[17,18]

The top-left panel in Fig. 3 shows the perpendicular electric field associated with the jet during injection 1. The electric field is characterized by intense fluctuations in the leading edge of the jet (345.150–345.155 s) and a strong reduction in the diamagnetic cavity associated with the dense plasma jet. This is consistent with depletion in the magnetic field associated with the plasma jet. The magnitude of the electric field prior to and after the cavity represents a jet $\boldsymbol{E} \times \boldsymbol{B}$ velocity of 25 km/s. The electric field recorded during the second injection is shown in Fig. 3 (top-right panel). Again, strong electric field fluctuations are observed in the leading edge of the jet. However, there is no observed decrease in the magnetic field associated with the core of the jet. This is consistent with the lower plasma-jet density and corresponding absence of a diamagnetic cavity. A more detailed discussion of the electric fields and plasma waves is provided by Pfaff et al.[19]

Ion and Electron Energy Flux

Ion and electron electrostatic analyzers were used to detect ions and electrons during the two injections (Fig. 4). The figure contains electron and ion energy flux data, with injection 1 on the left and injection 2 is on the right. Each panel shows the color-coded flux, integrated over the instruments' entire energy range (10–420 eV for ions and 0.01–10 keV for electrons), as a function of detector number vs time. The detectors are spaced azimuthally in order to obtain nearly complete two-dimensional coverage; see Lynch et al. for instrument details.[20] During injection 1, the core of the ion flux was observed parallel to the jet (see ion detector 8 in Fig. 4), although initially the ion flux was observed over a broad range of pitch angles. An enhanced electron flux was observed at all pitch angles with a slight enhancement in the direction parallel (electron detector 8) and antiparallel (electron detectors 1 and 15) to the jet. The electron detector was saturated from 345.16 to 345.28 s. The electron flux enhancement was observed before the ions during injection 1, perhaps because of the intense ultraviolet light from the ETG.

Plasma-jet ion flux in the direction of the jet was also detected during the ETG-2 injection (Fig. 4, right panel). The orientation of the PDP was different during injection 2 because of an increase in the coning angle of the payload. Nonetheless, the ion jet was recorded in detector 5. The ion energy flux was lower during the ETG-2 injection than during ETG-1 injection. The lower ion number flux is consistent with the Langmuir-probe observations showing the plasma jet density was two orders of magnitude smaller during injection 2. The electron flux from the jet was also observed during the ETG-2 injection. In this case, the detector did not saturate. In fact, a weak electron flux was observed in detectors 3 and 4 (from the direction of the jet) and later in detector 11 (in direction antiparallel to the jet).

Optical Emissions

An extensive array of ground-based and in situ sensors, as well as sensors on the MSX satellite, successfully recorded the optical signature of the plasma-jet injections (Tables 3 and 4). A mosaic of visible images acquired by the Poker Flat Situation camera separated by 0.016 s is shown in Fig. 5. During ETG-1, a somewhat spherical cloud was observed optically. In contrast, during ETG-2 the jet was elongated in the direction parallel to the magnetic field. At 0.15 s, the plasma jet appears to change direction. As a point of reference, these

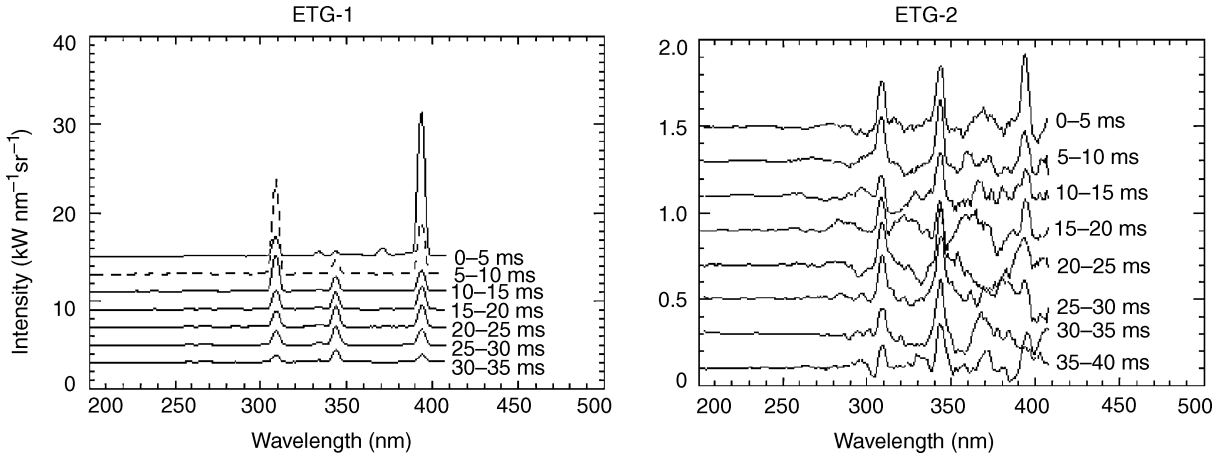

Fig. 5 Mosaic of visible images from the SIT camera for a) injection 1 and b) injection 2. The camera was located at Poker Flat, Alaska. The images progress in time from left to right.

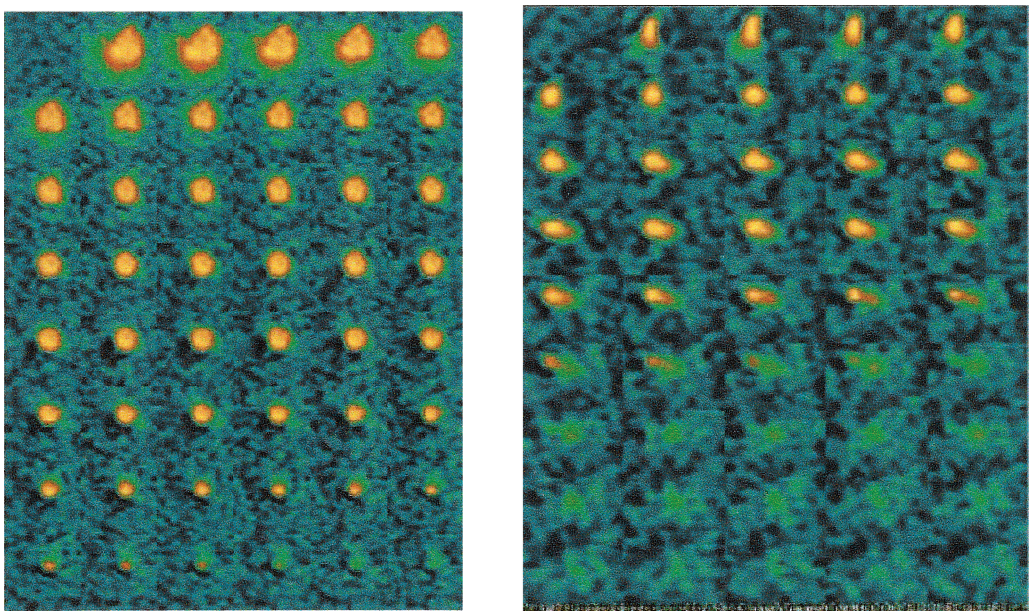

Fig. 6 Ultraviolet spectra acquired by OSP spectrograph during a) injection 1 and b) injection 2. The different traces show the spectrum at different times relative to the injection.

images correspond to times after the jet has passed the payloads and represent long-term effects caused by jet-space environment interaction. The size of the cloud is similar during both injections and reaches ∼5 km in diameter. One of the intensified charge-coupled device (ICCD) cameras at Kaktovik was used to observe artificial aurora. This camera viewed the plasma-jet field line footprint at 110-km altitude. Artificial aurora was not observed, possibly because of the presence of thin clouds at the time of the event.

Two spectrographs on the OSP were used to record ultraviolet and visible emissions during the plasma jet injection. Figure 6 shows spectra from the ultraviolet spectrograph. These spectra were collected at 5-ms intervals. Emissions lines in the ultraviolet were observed during both injections. The strongest emissions were recorded during injection 1. The spectral lines shown in Fig. 6 were caused by neutral aluminum, consistent with the fact that the jet was an aluminum ion jet. The lines generally started out strong and became weaker (310 and 395 nm), except in the case of the line near 345 nm, which was strongest around 20–25 ms. The presence of aluminum spectral features in the jet was also detected by the spectrographs on the MSX satellite during the North Star mission (data not shown) and are similar to the spectra recorded during the earlier Fluxus experiments.[13]

The PDP contained forward- and aft-looking photometers. The forward-looking photometer measured the injection time (from the initial flash), while the aft-looking photometer observed the jet as it passed the payload. The data (not shown) from the two photometers (380–420-nm band), both with a 30-deg field of view, indicate the radiating portion of the jet traveled at an average speed of 22 km/s from the jet source to the PDP location.

Summary

The North Star mission investigated the particle, field, and optical emission environment during two plasma jet injections. The observations during the North Star mission revealed significant differences between the ETG-1 and ETG-2 injections. These differences can be attributed to the presence of an artificial air cloud released prior to the ETG-1 injection and not present during the ETG-2 injection. This air cloud resulted in greater ionization of the high-speed aluminum neutrals in the jet as it interacted with the air cloud. In fact, the ETG device produces a highly ionized jet at very early times ($t < 1 \times 10^{-6}$ s), but these ions recombine to form a weakly ionized jet that includes a high-speed stream of neutrals. The flow of high-speed neutrals through the air cloud resulted in ionization

perhaps by the process of charge exchange ionization or by anomalous ionization resulting from the CIV process, discussed in more detail by Lynch et al.[20]

The magnetic perturbations and the diamagnetic cavity observed were successfully correlated with the observed plasma density. Gavrilov et al.[16] obtained a good comparison between the energy density of the jet and the observed diamagnetic cavity. The single-fluid, magnetohydrodynamic modeling of the ETG-1 injection conducted by Gatsonis et al.[17] shows the development of a diamagnetic cavity that compares well with the PDP observations. In addition, Gatsonis et al. show that the magnetic perturbations that emanate from the jet are three dimensional in nature and that observations on the payloads are thus sensitive to the orientation of the jet.

The current coupling between the jet and the ambient plasma is explored by Gatsonis et al.[17] with a single-fluid formulation and by Delamere et al.[18] with a hybrid (particle-fluid) formulation. Although the underlying models for currents are different in the two approaches, the emerging picture is one of a plasma jet that imparts momentum to the ambient, inducing motion and waves that travel into the background, thus slowing down. Gavrilov et al.[16] estimate that the jet did not slow down as fast as expected and attributed this result to the presence of the neutral component of the jet, which might be caused by inertia in the high-speed stream of the jet's neutral component.

The data analysis and modeling of the North Star mission provided significant insight and improved our understanding of complex far-field interactions between a plasma jet and magnetized plasma. The North Star plasma jets were similar in their characteristics to plumes from electric propulsion devices and plasmas resulting from the release of neutrals from onboard chemical thrusters. The North Star mission, therefore, provides a comprehensive view of the particle, field, and optical environment induced in the far field of an active spacecraft.

Acknowledgments

We thank the Active Plasma Experiment (APEX) North Star engineering team, the APEX North Star Applied Physics Laboratory management team led by Peter Partridge, and our Russian colleagues for their dedication to this project.

References

[1]Boyd, I. D., and Ketsdever, A. (eds.), "Special Section: Interactions Between Spacecraft and Thruster Plumes," *Journal of Spacecraft and Rockets*, Vol. 38, No. 3, 2001, pp. 380–464.

[2]Adushkin, V. V., Zetzer, J. I., Kiselev, Y. N., Nenchinov, I. V., and Christoforov, B. D., "Active Geophysical Rocket Experiments in the Ionosphere with the High Velocity Plasma Jet Injection," *Doclady RAS*, Vol. 331, No. 4, 1993, pp. 486–489.

[3]Haerendel, G., and Sagdeev, R. Z., "Artificial Plasma Jet in the Ionosphere," *Advances in Space Research*, Vol. 1, No. 2, 1981, pp. 29–46.

[4]Arnoldy, R. L., Cahill, L. J., Jr., Kintner, P. M., Moore, T. E., and Pollock, C. J., "Plasma Effects of Active Ion Beam Injections in the Ionosphere at Rocket Altitudes," *Advances in Space Research*, Vol. 12, No. 12, 1992, pp. 1–7.

[5]Kaufmann, R. L., Arnoldy, R. L., Moore, T. E., Kintner, P. M., Cahill, L. J., Jr., and Walker, D. N., "Heavy Ion Beam-Ionosphere Interactions: Electron Acceleration," *Journal of Geophysical Research*, Vol. 90, No. A10, 1985, pp. 9595–9614.

[6]Erlandson, R. E., Cahill, L. J., Jr., Pollock, C. J., Arnoldy, R. L., Scales, W. A., and Kintner, P. M., "Initial Results from the Operation of Two Argon Ion Generators in the Auroral Ionosphere," *Journal of Geophysical Research*, Vol. 92, No. A5, 1987, pp. 4601–4616.

[7]Pollock, C. J., Arnoldy, R. L., Erlandson, R. E., and Cahill, L. J., Jr., "Observations of the Plasma Environment During an Active Ionospheric Ion Beam Experiment," *Journal of Geophysical Research*, Vol. 93, No. A10, 1988, pp. 11473–11493.

[8]Torbert, R. B., Kletzing, C. A., Liou, K., and Rau, D., "Prompt Ionization in the CRIT II Barium Releases," *Geophysical Research Letters*, Vol. 19, No. 10, 1992, pp. 973–976.

[9]Swenson, G. R., Mende, S. B., Meyerott, R. E., and Rairden, R. L., "Charge Exchange Contamination of CRIT II Barium CIV Experiment," *Geophysical Research Letters*, Vol. 18, No. 3, 1991, pp. 401–404.

[10]Zetzer, J. I., Kozlov, S. I., Rybakov, V. A., Ponomarenko, A. V., Smirnova, N. V., Romanovsky, Y. A., Meng, C.-I., Erlandson, R., and Stoyanov, B., "Airglow in the Visible and Infrared Spectral Ranges of the Disturbed Upper Atmosphere Under Conditions of High-Velocity Plasma Jet Injection: I. Experimental Data," *Cosmic Research*, Vol. 40, No. 3, 2002, pp. 233–240.

[11]Gavrilov, B. G., Podgorny, A. I., Podgorny, I. M., Sobyanin, D. B., Zetzer, J. I., Erlandson, R. E., Meng, C.-I., and Stoyanov, B. J., "Diamagnetic Effect Produced by the Fluxus-1 and -2 Artificial Plasma Jet," *Geophysical Research Letters*, Vol. 26, No. 11, 1999, pp. 1549–1552.

[12]Mill, J. D., O'Neil, R. R., Price, S., Romick, J. I., Uy, O. M., and Gaposchkin, E. M., "Midcourse Space Experiment: Introduction to the Spacecraft, Instruments and Scientific Objectives," *Journal of Spacecraft and Rockets*, Vol. 31, No. 5, 1994, pp. 900–907.

[13]Erlandson, R. E., Swaminathan, P. K., Meng, C.-I., Stoyanov, B. J., Zetzer, J. I., Gavrilov, B. G., Kiselev, Y. N., and Romanovsky, Y. A., "Observation of Auroral Emissions Induced by Artificial Plasma Jets," *Geophysical Research Letters*, Vol. 26, No. 11, 1999, pp. 1553–1556.

[14]Erlandson, R. E., Meng, C.-I., Zetzer, J. I., Kiselev, Y., Gavrilov, B. G., Stenbaek-Nielsen, H., Lynch, K. A., Pfaff, R. F., Jr., Swaminathan, P. K., Dogra, V. K., Stoyanov, B. J., Delamere, P. A., Bounds, S., and Gatsonis, N. A., "The APEX North Star Experiment: Observations of High-Speed Plasma Jets Injected Perpendicular to the Magnetic Field," *Advances in Space Research*, Vol. 29, No. 9, 2002, pp. 1317–1326.

[15]Carbary, J. F., Darlington, E. H., Harris, T. J., McEvaddy, P. J., Mayr, M. R., Peacock, K., and Meng, C.-I., "Ultraviolet and Visible Imaging and Spectrographic Imaging Instrument," *Applied Optics*, Vol. 33, No. 19, 1994, pp. 4201–4213.

[16]Gavrilov, B. G., Podgorny, I. M., Sobyanin, D. B., Zetzer, J. I., Erlandson, R. E., Meng, C. I., Pfaff, R. F., and Lynch, K. A., "North Star Plasma-Jet Experiment Particles and Electric and Magnetic Field Measurements," *Journal of Spacecraft and Rockets*, Vol. 41, No. 4, 2004, pp. 490–495.

[17]Gatsonis, N. A., DeMagistris, M., and Erlandson, R. E., "Three-Dimensional Magnetohydrodynamic Modeling of Plasma Jets in North Star Space Experiment," *Journal of Spacecraft and Rockets*, Vol. 41, No. 4, 2004, pp. 509–520.

[18]Delamere, P. A., Stenbaek-Nielsen, H. C., Pfaff, R. F., Erlandson, R. E., Meng, C. I., Zetzer, J. I., Kiselev, Y., and Gavrilov, B. G., "Dynamics of the Active Plasma Experiment North Star Artificial Plasma Jet," *Journal of Spacecraft and Rockets*, Vol. 41, No. 4, 2004, pp. 503–508.

[19]Pfaff, R. F., Freudenreich, H. T., Bounds, S., Delamere, P. A., Erlandson, R. E., Meng, C. I., Zetzer, J. I., and Gavrilov, B. G., "Electric Field, Magnetic Field, and Density Measurements on the Active Plasma Experiment," *Journal of Spacecraft and Rockets*, Vol. 41, No. 4, 2004, pp. 521–532.

[20]Lynch, K. A., Torbert, R. B., Chutter, M., Erlandson, R. E., Meng, C. I., Zetzer, J. I., Gavrilov, B. G., and Kiselev, Y., "Active Plasma Experiment: North Star Particle Data," *Journal of Spacecraft and Rockets*, Vol. 41, No. 4, 2004, pp. 496–502.

D. L. Cooke
Guest Editor